Ab initio molecular dynamics simulation of a medium-sized water cluster anion: from an interior to a surface located excess electron via a delocalized state

Tomaso Frigato[†], Joost VandeVondele[‡], Burkhard Schmidt[†],
Christof Schütte[†], Pavel Jungwirth[‖*]

[†]Institut für Mathematik, Freie Universität Berlin,
Arnimallee 6, Berlin D-14195, Germany

[‡]Physical Chemistry Institute, Zürich University,
Winterthurerstrasse 190, CH-8057 Zürich, Switzerland

[‖]Institute of Organic Chemistry and Biochemistry,
Academy of Sciences of the Czech Republic
and Center for Biomolecules and Complex Molecular Systems,
Flemingovo nam. 2, 16610 Prague 6, Czech Republic

[*] e-mail: pavel.jungwirth@uochb.cas.cz

Abstract

We present a computational study of the structure and dynamics of an excess electron in a medium-sized water cluster aimed at addressing the question of interior vs. exterior solvation. Ab initio Born-Oppenheimer molecular dynamics simulations are performed within the DFT framework, employing a hybrid Gaussian and plane waves

formalism together with the PBE exchange-correlation functional and norm-conserving pseudopotentials. The analysis of a 15 ps trajectory allows us to reach the following conclusions: (i) the excess electron is predominantly located at the cluster surface (even if it is initially placed in the interior), (ii) the computed electron binding energies correlate with the electron localization rather than with its bulk vs surface location, (iii) a dynamical interconversion between two different H-bond patterns around the electron is found. The computed electron binding energies and the most relevant features of the IR spectrum are in a very good agreement with previous experimental studies.

1 Introduction

Excess electrons in water, denoted as hydrated electrons e^-_{aq}, are of fundamental importance in several fields including radiation and atmospheric chemistry, biology, and astrophysics [1, 2, 3], and have, therefore, been subject of large interest since their discovery in 1962 [4]. The ability to bind an electron is a collective property of water molecules: while a single water molecule does not bind an excess electron, a water dimer aready does [5]. However, the character of the excess electron in a water dimer and in small water clusters in general is different from that in the bulk. In small clusters the excess electron, commonly denoted as dipole bound electron, is weakly bound at the exterior by electrostatic and dispersion interactions [6, 7, 8, 9, 10, 11, 12, 13]. Its binding energy is in the 100 meV range and a relevant fraction of its wavefunction typically exceeds the size of the water cluster. In contrast, in larger clusters with tens to hundreds of water molecules the electron binding is stronger (in the eV range) being mainly of electrostatic nature [14, 15, 16, 17, 18, 19, 20], and its properties such as binding energy and solvation structure converge to those observed for hydrated electrons in extended aqueous systems.

Small anionic water clusters offer an appealing alternative to bulk systems, as experiments can be carried out under well controlled conditions, and simulations may be per-

formed with a sufficiently accurate methodology. Bulk properties can be extrapolated from the behaviour of clusters of increasing size. However, we stress an important issue concerning the extrapolation of cluster properties to the bulk liquid, namely temperature. Cluster experiments are typically carried out under cryogenic conditions, so the systems are either nanocrystals or amorphous. Consequently, one should be cautious when extrapolating to the situation of an electron in the bulk liquid.

Despite the numerous efforts, electron solvation in water cluster is still not completely understood. One of the most fundamental questions, whether the electron prefers interior solvation or surface solvation, is still a matter of controversy. Surface states were first identified by path integral molecular dynamics (MD) simulations [21] and the authors found out that surface states are preferred for cluster comprising of 8 to 32 water molecules. For $(H_2O)_n^-$ with $n \geq 64$, it was deduced that internal solvation becomes energetically favoured, implying a surface-to-bulk transition in the $32 \leq n \leq 64$ molecules range. Electron photodetachment experiments for clusters up to $n = 69$ [14] showed that the electron binding energy scales linearly with $n^{-1/3}$ for $n \geq 11$. This can be compatible with internally solvated electrons, as a simple theoretical model predicts the same scaling for a spherical charge distribution in a uniform dielectric medium [21].

An important experimental breakthrough was achieved recently [15]. Monitoring electron photo-detachment spectra of small clusters under different experimental conditions, typically at temperatures around 200 K where such clusters are belived to be still liquid-like, it was possible to demonstrate the co-presence of (at least) three different isomers. These isomers were characterized by different values of the electron vertical detachment energy (VDE), and the authors, on the basis of VDE scaling arguments and comparison with theoretical calculations, described the most stable isomer as a bulk state and the remaining two as surface states. Moreover, it was suggested that the expected surface-

to-bulk solvation transition takes place already for rather small clusters ($n \geq 11$). These claims, although supported by a later experimental work [16], have been challenged by quantum-classical pseudopotential simulations [17], in which the most stable state appears as a surface state, and the surface-to-bulk transition takes place for larger clusters. The authors of this computational study also refer to a different theoretical model that gives rise to a $n^{-1/3}$ scaling of VDEs for surface states as well [22]. However, recent high level ab initio minimizations [19] found internally solvated electrons already for water clusters with only 15 H_2O molecules (albeit for high energy isomers), so that the question of internal vs surface electron solvation in water clusters is not fully answered yet.

Regarding the solvation structure, particular attention has been paid to the local hydrogen-bonding motif around the excess electron. Especially in smaller clusters, deviations from the bulk solvation structure, where the electron is found inside a cavity surrounded by roughly six water molecules [23], can be expected. A red-shifted HOH bending band was experimentally observed for cluster up to $\sim$ 20 water molecule [10]. Ab initio calculations, which confirmed the experimental findings [9], indicate that this red shift derives from a strong charge transfer to the O-H σ^* orbital of a single water molecule. This water molecule points both its hydrogen atoms toward the electronic cloud in the so called double hydrogen-bond acceptor (AA) configuration. Vibrational spectra of cryogenic water clusters in the 15-50 molecules range [20] show that this motif is clearly observed for the smaller clusters, while its spectroscopic signature broadens with increasing cluster size, indicating a more delocalized electron binding structure. This brings an interesting question about the presence and relative stabilities of the cavity and single acceptor molecule structures.

Most previous dynamical simulations of hydrated electrons were performed using a pseudopotential approach. Within this method only the excess electron is treated as a

quantum mechanical particle, while the interactions between the classical water molecules and the excess electrons are described via an empirical pseudopotential [13, 17, 18, 21, 24, 25, 26, 27, 28]. By construction such models do not include many-electron effects, save for the recent Drude model study of water hexamer anion [13]. Exceptions to pseudopotential simulations are three studies of the bulk hydrated electron, two based on the Car-Parrinello MD [29, 30] and one employing a quantum-mechanics/molecular mechanics (QM/MM) approach [31], and a Car-Parrinello MD study of a surface trapped electron on ice [32]. It is worth mentioning that in Ref. [31] the authors explicitly stated that many-electron effects must accounted for in order to reproduce the charge transfer to the 2p orbitals of the oxygen atoms surrounding the electron, necessary to explain magnetic resonance results [33]. However, to the best of our knowledge all (valence) electron model have been considered only when simulating either the bulk hydrated electron [29, 30, 31, 32] or extremely small clusters (such as $(H_2O)_4^-$ [34]), but not medium-sized clusters where only one-electron model have been used [17, 18, 21].

The present study aims at filling this gap, providing all (valence) electron simulations of an excess electron in/on a medium-sized anionic water cluster $(H_2O)_{32}^-$. In particular, we aim at providing answers to the following questions: i) Does the excess electron prefer surface or interior configurations in medium-sized liquid-like water clusters? ii) How does the electron binding energy correlate with its delocalization and location in the cluster and how do the calculated values relate to those from photoelectron spectroscopy? iii) How do water molecules arrange around the excess electron and is the AA motif, found in cryogenic clusters, preserved in the liquid phase? iv) What are the signatures of electron binding in the vibrational spectrum of the cluster? v) How accurately does the Density Functional Theory (DFT) employed in the simulations (i.e., the PBE functional) describe the structure and dynamics of the hydrated electron?

At ambient conditions, the chosen intermediate cluster size ensures the following. On one hand, the system is small enough that the ab initio simulations are sufficiently efficient to allow for reasonable statistics, while on the other hand, it is big enough to make internal electron solvation principally possible. Even smaller clusters have been shown to be able to accommodate an internally located electron [19]; however, a larger cluster was chosen here for two reasons. The electron binding energy is closer to the bulk value and the dispersion interaction (not accounted for at the DFT level used throughout the simulations), the relative contribution of which decreases with cluster size, is less important for the present system than for small clusters.

2 Methods

Ab initio molecular dynamics simulations were performed using the public domain computer code CP2K [35]. In its electronic structure module, calculations are performed at the DFT level within the hybrid Gaussian and plane waves method GPW [36] and the electronic ground state density is converged at each step (the so called Born-Oppenheimer dynamics). Kohn-Sham orbitals are expanded into atom-centered gaussian types orbital functions, while the electron density is represented with an auxiliary plane waves basis.

A simulation setup very similar to that previously successfully applied to liquid water simulations was chosen [36, 37]. Core electrons were removed by the introduction of norm conserving pseudopotentials developed by Goedecker, Teter and Hutter (GTH [38]), and a charge density cutoff of 280 Ry was used for the auxiliary basis set. The Perdew-Burke-Ernzerhof (PBE) exchange-correlation functional was used [39], since it yields similar behaviour of liquid water when compared with the more often employed BLYP functional [40], however, with a lower vapor pressure and consequently more stable clusters [41]. Kohn-Sham orbitals were expanded into a triple zeta valence basis, with the addition of very

diffuse functions, which are particularly important for proper description of configurations where the electron is localized on the cluster surface. This basis set, denoted as m-TZV2P, in described in detail in Ref. [42].

As plane waves are intrinsically periodic, simulations of isolated systems are only possible with the introduction of a cluster correction term [43] and a unit cell at least twice as large as the simulated system (including the electronic density). Therefore, the water cluster was placed in the middle of a cubic box with a size of 20 Å. The system was coupled via a Nose-Hoover thermostat to a bath at T=350 K, to enhance sampling and ensure liquid behavior [37, 40, 44]. Deuterated water was used, and equations of motion were integrated with a 0.5 fs timestep.

To estimate the accuracy of the electronic structure calculations performed during the Born-Oppenheimer MD run, higher level calculations were performed on a small subset of configurations extracted from the simulated trajectory. First, the effect of the spurious self interaction energy present in DFT calculations was investigated. It is known that in systems with unpaired electrons the self interaction error present in DFT calculations may lead to inaccurate results [32, 45]. However, it has been shown previously that for a bulk hydrated electron this does not seem to be the case and inclusion of self-interaction corrections (SIC) terms does not significantly modify the results [30]. A similar behaviour was, therefore, expected in our calculations, nevertheless we checked for the possible effects of self interaction. The SIC term used was taken from Ref. [46]; $E_{sic} = -aE_H[m] - bE_{XC}[m, 0]$, where m is the system total spin density, $E_H[m]$ the Hartree and $E_{XC}[m, 0]$ the exchange-correlation functional. For the parameters of this empirical correction, we followed Ref. [46] and set $a = 0.2$ and $b = 0$.

Next, the accuracy of the PBE functional used was checked by comparing for representative cluster geometries along the MD trajectory energies and spin densities extracted

from the simulation with those calculated at the B3LYP/6-31++G** [47, 48, 49] and RIMP2/aug-cc-pVDZ [50, 51, 52] levels. As shown in Ref. [53], MP2 calculations, with the use of sufficiently diffuse functions, reach for small ($n \leq 4$) electron-water clusters a 0.05 eV accuracy when compared with experimental and coupled cluster theory results representing, therefore, quite a reliable benchmark.

Besides the CP2K program, Gaussian03 [54] and Turbomole [55] V5.9 were used for ab initio single point energy calculations, and NWChem [56] for the classical molecular dynamics equilibration described in the next section. Electronic densities were plotted using the programs VMD [57] and gOpenMol [58, 59].

3 Results

3.1 Initial conditions

An initial configuration was built with the electron localized in the cluster interior using the following procedure. First, a system consisting of 32 water molecule with an auxiliary iodide anion was considered. A 500 ps classical molecular dynamics equilibration was performed using the AMBER empirical force field [60], in which the I^- van der Waals radius (2.35 Å) is close to the equilibrium value of the bulk hydrated electron radius (2.5-2.6 Å[31, 61, 62]). We can thus assume that the water structure around I^- will be similar to that around e^-. The system was coupled to a bath at T=250 K (the relatively low temperature allowed to prevent water molecules evaporation while still keeping the system liquid-like), and a 1 fs time-step was used for the integration of the equations of motion. The use of a non-polarizable empirical potential and short equilibration time resulted in I^- remaining prevalently located in the cluster interior [63]. A second stage of equilibration was found necessary to avoid spurious effects due to the abrupt switch between an empirical

force field and ab initio dynamics. Therefore, a configuration characterized by I^- located inside the water cluster was extracted from the last 10 ps of the equilibration simulation, and used as starting configuration for a short (2 ps) ab initio simulation at 350 K. This short simulation was performed with a basis set not including extra diffuse functions, to prevent the iodide ion from migration toward the cluster surface.

Once this equilibration procedure was completed, I^- resided in an internal cluster cavity suitable for accommodating an excess electron, as far as the cavity size and the orientation of surrounding water molecules are concerned. The auxiliary iodide anion was thus removed and replaced by an electron by simply setting the charge of the water cluster to -1 e. A final production run of 15 ps at 350 K was consequently performed with the m-TZV2P basis set (i.e., with the very diffuse functions).

3.2 Bulk versus surface solvation

Three principle observables were monitored during the 15 ps production run at regular 20 fs intervals:

1. The system VDE (which is except for the sign the vertical binding energy of the excess electron), computed as $VDE = E[(H_2O)_{32}] - E[(H_2O)_{32}^-]$ with both energies evaluated at the anionic geometry.

2. The degree of localization of the excess electron was expressed as its radius of gyration $R_e = \sqrt{\frac{\int \rho(\mathbf{x})(\mathbf{x}-\mathbf{x_{el}})^2 d\mathbf{x}}{\int \rho(\mathbf{x}) d\mathbf{x}}}$, where $\rho(\mathbf{x})$ is the excess electron density with its center of mass at $\mathbf{x_{el}} = \frac{\int \rho(\mathbf{x}) \mathbf{x} d\mathbf{x}}{\int \rho(\mathbf{x}) d\mathbf{x}}$.

3. As a measure of the distance between the cluster geometrical center $\mathbf{x_{aq}}$ and the excess electron we monitored the quantity $R_d = \frac{\int \rho(\mathbf{x})(|\mathbf{x}-\mathbf{x_{aq}}|) d\mathbf{x}}{\int \rho(\mathbf{x}) d\mathbf{x}}$.

The choice of considering the system spin density instead of the highest occupied molecular orbital (HOMO) for representing the excess electron, was determined by the fact that the spin density is a measurable quantity, in contrast to molecular orbitals. Besides, Kohn-Sham orbitals do not have a direct correspondence with molecular orbitals. We verified that in the electron-water cluster the spin density overlaps very well with the differential electronic density (i.e., the difference between electron densities of the anionic and neutral systems in the anionic geometry), although the latter is somewhat more diffuse. Therefore, in the following, we refer to the spin density as to the excess electron density.

The three computed quantities along the MD trajectory are shown in Fig. 1. Due to the fact that the cluster was prepared with the interior cavity, e^-_{aq} is first localized inside the water cluster, as can be deduced from the excess electron density plot and the smaller value of R_d. After about 0.5 ps, electron delocalization starts, and a maximum R_e value of about 5 Å is reached after $\sim$1.5 ps. As can be seen from the spin density isosurface in Fig. 1, the electron is now mainly localized at two opposite cluster sides, with smaller values of the spin density observed all over the cluster. Finally, the electron radius starts to shrink again. At the end of the localization process (t $\sim$3 ps) the electron is found at the cluster surface (with R_d displaying higher values compared to the beginning of the simulation). This surface state appears to be relatively stable for 6 ps. Then, a brief delocalization phase is observed, followed again by electron localization on the cluster surface. Note that during the delocalization phases the electron remains predominantly at the cluster surface with the two main density lobes located at opposite sides of the cluster.

It is instructive to evaluate the average electron radius of gyration R_{av}. We get R_{av} = 3.24 Å when the whole trajectory is considered, while R_{av} = 2.90 Å when we remove the trajectory segments with a very delocalized electron (0 $ps < t <$ 3 ps and 9 $ps < t <$ 11 ps). Note that this value is only about 10 % larger than the radius of gyration of a bulk solvated

electron.

A quantitive criterion for distinguishing between internal and external states was introduced in Ref. [17]; the electron is considered to be internally solvated when the distance between its center and the cluster center plus its radius R_e is smaller that the cluster radius R_{cl}, i.e. $|\mathbf{x_{el}} - \mathbf{x_{aq}}| + R_e < R_{cl}$. According to this criterion, internally solvated electrons are found in less than 3% of snapshots from the present trajectory, all of them belonging either to the initial phase of the simulation or to the two delocalization events. For the remaining 97% of the trajectory the excess electron is localized at the surface of the cluster.

The distribution of VDE values for the whole the trajectory is depicted in Fig. 2. It is rather broad exhibiting a major peak at 1.6 eV (about half the value of excess electron binding in bulk water) and a side peak at around 0.7 eV. Larger VDEs are connected with more localized states, while smaller ones with more delocalized configurations of the excess electron. The VDE values thus closely correlate with the degree of electron localization rather than with its position within the cluster (see Fig. 3).

3.3 Solvation structure and IR spectrum

The IR vibrational spectrum was estimated as the Fourier transform of the velocity-velocity autocorrelation function, restricted only to the trajectory segment from t=3 to t=9 ps, characterized by a relatively stable surface located excess electron. Several evenly symmetrized time series of $t_{TOT}/2$ length (where t_{TOT} is the total length of the 6 ps segment) were obtained by shifting the time origin by 125 fs along the simulated trajectory. For every time series a discrete Fourier transform was performed in conjunction with a Blackman smoothing function [64]. The resulting spectrum shows three different bands (Fig. 4), corresponding to libration, intramolecular bending and stretching modes. We focus here on the H-O-H bending region, where the AA signature is expected as a red-shifted side peak.

Since the short length of the simulation does not allow to distinguish between the two peaks, which are expected to be separated by about 100 cm^{-1} [20], the IR spectrum was decomposed into three parts. The first one was obtained by restricting the computation of the velocity autocorrelation function to the water molecule closest to the electron center. Next, the second to sixth closest molecules were considered, while the last spectrum was computed as a contribution from the remaining 26 H_2O molecules. In Fig. 4 the three IR spectra are shown, focusing on the bending region. Although the spectra obtained from all molecules and from the 26 waters more distant from e^-_{aq} are quite similar to each other, the higher frequency peak at $1250\,cm^{-1}$ disappears when only the closest molecules are considered. The fact that in contrast the lower frequency peak at around $1130\,cm^{-1}$ persists even when only the closest water molecule to the excess electron indicates a possible occurrence of the AA motif.

Besides vibrational spectra, a simple geometrical criterion can yield additional information about e^-_{aq} solvation structure. We compare the average distance between the electron center and the two hydrogen atoms of the closest H_2O molecule to the excess electron with the same quantity averaged over the six closest molecules (Fig. 5). This allows us to identify geometries where several water molecules interact similarly with the excess electron (in this case the two curves show similar values) from AA-type structures. There, the approximate symmetry of the solvent shell is broken and a single molecule is found significantly closer to the excess electron than the others (therefore, the two curves come apart). From Fig. 5, we see that there are frequent interconversion between these two situations. Examining the excess electron density at t=6.12 ps, corresponding to a large difference between the two averaged distances, a clear AA motif is seen with one H_2O molecule located very close to the electron and pointing both hydrogen atoms toward the electronic cloud (Fig. 6). In contrast, a situation where the two curves in Fig. 5 are close to each other, like that

at t=6.62 ps, is characterized by several water molecules surrounding the excess electron, each donating it a single hydrogen bond (Fig. 7).

3.4 Comparison with higher level ab initio calculations

The accuracy of the DFT level of theory underlying the dynamical calculations was tested against benchmark calculations for representative snapshots extracted from the simulated trajectory. The analysis was restricted to the trajectory segment from t=0 to t=3 ps which covers all the important patterns investigated, i.e., interior, delocalized, and surface localized excess electrons. Single point calculations at PBE-GTH-m-TZV2P level with the self interaction correction were computed at regular 300 fs intervals. B3LYP/6-31++G** and RIMP2/aug-cc-pVDZ calculations which are rather costly were performed for several snapshots representing an internally localized, externally localized, and delocalized excess electron.

Fig. 8 summarizes the benchmarking results. First, note that the computed quantities are only weakly modified when the SIC term is included. The excess electron is somewhat more localized and VDE values are slightly higher when the self interaction error is removed, while the electron position R_d is basically left unchanged. Interestingly, the SIC term was found to be more important in simulations of an excess electron on ice [32]. In Ref. [32], one illustration of the importance of a SIC is a calculation of the electron affinity (EA) of a single water molecule. The reported value for an uncorrected BLYP calculation is 1 eV, while a SIC calculation yields a vanishing EA, in agreement with experiment. The large EA obtained with a standard GGA is a surprising result, which we have tried to reproduce. Calculating the EA of a nearly unbound, and thus very diffuse electron is not straightforward. Calculations based on Gaussian basis sets require very diffuse functions [65], while plane wave calculations require very large unit cells, and proper boundary

conditions (i.e. non-periodic) for the electrostatic calculations. We note that the electron affinity computed using periodic boundary conditions depends on the conventional zero of the potential, and that a SIC might change that convention. Here, we have employed a cubic unit cell with 40 Å edges, non-periodic boundary conditions and a TZV2PX basis, for Oxygen augmented with 10 sets of diffuse s and p functions with common exponents ranging from 0.16 to 0.0003125 in a geometric progression. With this setup, we find an EA less than 0.1eV and suggest that this value will converge to ∼0 eV (in agreement with experiment; calculations may actually still show a marginal binding of the electron due to the use of the Born-Oppenheimer approximation) for even larger unit cells. This result is obtained without the need to resort to a SIC correction.

B3LYP results are also in a very good agreement with values extracted from the MD simulations, with the observed transition from an internally localized to an externally localized electron taking place via the same delocalized electron state. There, the excess electron is slightly more delocalized and further away from the cluster center at the B3LYP level. Comparison with our most accurate RIMP2/aug-cc-pVDZ level of theory is revealing. In full agreement with DFT results, RIMP2 calculations yield an internally localized electron for the first snapshot considered and an externally localized electron for the last case, with both R_e and R_d values being well reproduced. Moreover, VDEs at the RIMP2 level are in very good agreement with the PBE-GTH-m-TZV2P values. The transition from internal to external excess electron occurs via a delocalized state at the RIMP2 level, too. However, as can be seen from R_e and R_d values computed for intermediate configurations, a shorter delocalized phase is observed at the RIMP2 level, with the electron being pushed faster and further away from the cluster center compared to all DFT calculations.

As a check of basis set convergence, we added additional diffuse functions centered at the atom closest to the electron center of mass (2 sets of diffuse s and p functions

sharing the same exponents 0.015 and 0.003) for two selected geometries, one (t=1.2 ps) corresponding to a very delocalized excess electron, and the other (t=3 ps) corresponding to a localized surface electron. In both cases the change in binding energy was found to be small (< 0.1 eV). Additionally, we verified the vanishing difference between spin and differential electronic densities. This difference is very small both at RIMP2 and PBE-GTH-m-TZV2P levels. Fig. 9 shows how the two densities coincides, with the differential density being slightly more diffuse.

In conclusion, the PBE-GTH-m-TZV2P method performs very well for the description of both interior and surface localized excess electrons. However, it tends to overestimate the delocalization and timescale connected with the bulk-to-surface transition of the excess electron.

4 Discussion

The present calculations provide data that can be related to various experimental observables. First, however, one should be aware of the fact that it is in principle possible that a more stable structure, characterized by an internally solvated electron, may exist in case it has a very different structure than $I^-(H_2O)_{32}$, and the two structures are separated by a very large energy barrier, that cannot be overcome due to the limited length of our simulations. Anyway, previous theoretical and experimental research, summarized below, does not not seem to support this hypothesis, confirming our findings.

A direct contact with experiments is obtained comparing the VDEs with electron photodetachment spectra [14, 15]. In Fig. 2 two peaks are born from our VDE distribution. This is superficially similar to a recent experimental result [15], where the lower energy peak is assigned to a surface state and the second one to a bulk state. However, noticing the lack of correlation between the calculated VDEs and the excess electron position R_d

(top panel in Fig. 3), while observing the strong inverse relationship between VDE and the electron radius of gyration (lower panel in Fig. 3), leads us to a different interpretation of the spectrum. The lower VDE peak corresponds to a strongly delocalized e^-_{aq}, while the higher energy peak reflects a localized excess electron. For the most of our trajectory the latter corresponds to a surface state, however, the initial internally localized electron state has a similar binding strength as the final surface state. Therefore, it also contributes (albeit marginally) to the higher energy peak in the VDE spectrum. The bottom line is that the value of VDE characterizes the degree of localization of the excess electron rather than its position within the cluster.

A second contact to experimental observables is via the IR spectrum. Note, however, that deuterated water was used in the simulations, which explains the shift between the simulated and measured vibrational peaks. It was recently observed that the AA motif of a single strongly interacting water molecule, characterized by a red-shifted peak in the bending region, is observed even for relatively large cluster (n $\sim$ 50) [20]. As the cluster size further increases this peak merges with the signal from water molecules not interacting so strongly with the excess electron. By decomposing the calculated IR spectrum into contributions from molecules at different distances from e^-_{aq} and using a simple geometrical criterion, it was possible to deduce that dynamical interconversions between AA and cavity structures occur. Such structures were also clearly recognized from the excess electron density plots.

Regarding comparison with other theoretical calculations, two previous studies concluded that for clusters of the present size electron surface solvation is favoured over internal solvation [17, 21]. This is in agreement with the present results. Quantitatively, compared to these one-electron pseudopotential calculations [17], where a large average electron radius R_{av} was observed for the surface state (for $n = 30$, R_{av} larger than 4 Å),

our estimate of $R_{av} = 3.23$ Å is smaller, and thus closer to the bulk hydrated electron value.

5 Conclusions

We performed a 15 ps long ab initio MD simulation of a $(H_2O)_{32}^-$ cluster. By construction the excess electron was initially located in the cluster interior. However, during the dynamics the electron moves rapidly to the cluster surface within a $\sim$ 2 ps long transient phase characterized by a delocalized state. The electron then remains at the cluster surface for the rest of the simulated trajectory, its radius of gyration being most of the time only slightly larger than its equilibrium bulk value. Therefore, we can confirm that for water clusters of the size examined here surface solvation is favoured by the excess electron over an internal state. For interpretation of photoelectron spectra it is important to note that the calculated VDE values did not show a correlation with the electron position within the cluster, however, a very strong correlation was found between the electron radius of gyration and its binding energy. A geometrical analysis of the solvation shell of the excess electron showed that two structures frequently interconvert. The first one has several water molecules interacting in a similar way with the electron, while in the second one a single water molecule moves closer to the electronic cloud [9, 10]. The computed IR spectrum, decomposed into contributions from different water molecules, confirmed this finding, as well as the repeated temporal presence of the AA binding motif of a single strongly bound water molecule [20]. Finally, we note that the PBE level of the DFT theory used for the MD electronic structure calculations compared well with benchmark calculations. Namely, it was found that VDE values along the trajectory are in very good agreement with accurate RIMP2 predictions. When the electron is localized at the surface (or initially in the interior) the excess electron size and location are also accurately reproduced. Only

in the transient phase, characterized by a very delocalized excess electron, the degree of delocalization is overestimated within all DFT methods employed.

6 Acknowledgments

P.J. acknowledges support from the Czech Ministry of Education (grant LC 512) and the Granting Agency of the Czech Republic (grant 202/06/0286). A part of the presented calculations has been performed on the HLRN supercomputer. We thank Dr. Knut Asmis for very interesting discussions.

References

[1] *Excess electrons in Dielectric Media*, edited by C. Ferradini and J.-P. Jay-Gerin (CRC, Boca Raton, FL, 1991)

[2] Lu, Q. B.; Sanche, L. *Phys. Rev. Lett.*, **2001**, *87*, 078501.

[3] Lu, Q. B.; Sanche, L. *Phys. Rev. B*, **2001**, *63*, 153403.

[4] Hart, E. J.; Boag, J. W. *J. Am. Chem. Soc.*, **1962**, *84*, 4090.

[5] Tsurusawa, T.; Iwata, S. *Chem. Phys. Lett.*, **1998**, *287*, 553.

[6] Tachikawa, H. *J. Chem. Phys.*, **2006**, *125*, 144307.

[7] Clary, D. C.; Benoit, D. M. *J. Chem. Phys.*, **1999**, *111*, 10559.

[8] Smith, D. M. A.; Smets, J., Elkadi, Y.; Adamowicz, L. *J. Chem. Phys.*, **1998**, *109*, 1238.

[9] Herbert, J. M.; Head-Gordon, M. *J. Am. Chem. Soc.*, **2006**, *128*, 13932.

[10] Riscioli, J. R.; Hammer, N. I.; Johnson, M. A. *J. Phys. Chem. A*, **2006**, *110*, 7517.

[11] Sommerfeld, T.; Jordan, K. D. *J. Phys. Chem. A*, **2006**, *109*, 11531.

[12] Wang, F.; Jordan, K. D. *J. Chem. Phys.*, **2002**, *116*, 6973.

[13] Sommerfeld, T.; Gardner, S. D.; DeFusco A; Jordan, K. D. *J. Chem. Phys.*, **2007**, *125*, 174301.

[14] Coe, J. V.; Lee, G. H.; Eaton, J. G.; Arnold, S. T.; Sarkas, H. W.; Bowen, K. H.; Ludewigt, C.; Haberland, H.; Worsnop, D. R. *J. Chem. Phys.*, **1990**, *92*, 3980.

[15] Verlet, J. R. R.; Bragg, A. E.; Kammrath, A.; Cheshnovsky, O.; Neumark, D. M. *Science*, 307, 93 (2005).

[16] Coe, J. V.; Arnold, S. T.; Eaton, J. G; Lee, G. H.; Bowen, K. H. *J. Chem. Phys.*, **2006**, *125*, 014315.

[17] Turi, L.; Sheu, W. S.; Rossky, P. J. *Science*, **2005**, *309*, 914.

[18] Turi, L.; Madarasz, A.; Rossky, P. J. *J. Chem. Phys.*, **2006**, *125*, 014308.

[19] Khan, A. *J. Chem. Phys.*, **2006**, *125*, 024307.

[20] Asmis, K. R.; Santambrogio, G.; Zhou, J.; Garand, E.; Headrick, J.; Goebbert, D.; Johnson, M. A.; Neumark, D. M. *J. Chem. Phys.*, **2007**, *126*, 191105.

[21] Barnett, R. N.; Landman, U.; Cleveland, C. L.; Jortner, J. *J. Chem. Phys.*, **1988**, *88*, 4429.

[22] Makov, G.; Nitzan, A. *J. Phys. Chem.*, **1994**, *98*, 3459.

[23] Tauber, M. J; Mathies, R. A. *J. Am. Chem. Soc.*, **2003**, *125*, 1394.

[24] Rossky, P. J.; Schnitker, J. *J. Phys. Chem.*, **1988**, *92*, 4277.

[25] Schnitker, J.; Motakabbir, K.; Rossky, P. J.; Friesner, R. *Phys. Rev. Lett.*, **1988**, *60*, 456.

[26] Skorobogatiy, M.; Park, I. J.; Joannopolous, J. D. *Comp. Mat. Sci.*, **2005**, *32*, 96.

[27] Boutin, A.; Spezia, R.; Coudert, F.; Mostafavi, M. *Chem. Phys. Lett.* , **2005**, *409*, 219.

[28] Turi, L.; Borgis, D. *J. Chem. Phys.*, **2002**, *117*, 6186.

[29] Boero, M.; Parrinello, M.; Terakura, K.; Ikeshoji, T.; Liew, C. C. *Phys. Rev. Lett.*, **2003**, *90*, 226403.

[30] Boero, M. *J. Phys. Chem. A*, **2007**, published online, DOI: 0.1021/jp074356+.

[31] Shkrob, I. A.; Glover, W. J.; Larsen, R. E.; Schwartz, B. J. *J. Phys. Chem. A*, **2007**, *111*, 5232.

[32] Baletto, F.; Cavazzoni, C.; Scandolo, S. *Phys. Rev. Lett.* , **2005**, *95*, 176801.

[33] Shkrob, I. A. *J. Phys. Chem. A*, **2007**, *111*, 5223.

[34] Herbert, J. M.; Johnson, M. A. *Prot. Nat. Acad. Sc.*, **2006**, *103*, 14282.

[35] The CP2K developers group, http://cp2k.berlios.de, **2004**.

[36] VandeVondele, J.; Krack, J.; Mohammed, F.; Parrinello, M.; Chassaing, T.; Hütter, J. *Comp. Phys. Comm.*, **2005**, *167*, 103 .

[37] Kuo, I. W.; Mundy, C. J.; McGrath, M. J.; Siepmann, J. I.; VandeVondele, J.; Hutter, J.; Sprik, M.; Hutter, J.; Chen, B.; Klein, M.; Mohammed, F.; Krack, M.; Parrinello, M. *J. Phys. Chem. B*, **2004**, *108*, 12990.

[38] Goedecker, S.; Teter, M.; Hutter, J. *Phys. Rev. B*, **1996**, *54*, 1703.

[39] Perdew, J. P.; Burke, K.; Ernzerhof, M.; *Phys. Rev. Lett.*, **1996**, *77*, 3865.

[40] VandeVondele, J.; Mohammed, F.; Krack, M.; Hütter, J.; Sprik, M.; Parrinello, M. *J. Chem. Phys.*, **2005**, *122* 014515.

[41] McGrath, M. J. ; Siepmann, J. I.; Kuo, I. F. W.; Mundy, C. J. *Mol. Phys.*, **2006**, *104*, 3619.

[42] VandeVondele, J. ; Hutter, J. *J. Chem. Phys.*, **2007**, *127*, 114105.

[43] Martyna, G.; Tuckermann, M.; *J. Chem. Phys.*, **1999**, *100*, 2810.

[44] Schwegler, E.; Grossman, J. C.; Gygi, F.; Galli. G. *J. Chem. Phys.*, **2004**, *121*, 5400.

[45] Gräfenstein, J.; Kraka, E.; Cremer, D. *Phys. Chem. Chem. Phys.*, **2004**, *6*, 1096.

[46] VandeVondele, J.; Sprik, M. *Phys. Chem. Chem. Phys.*, **2005**, *7*, 1363.

[47] Becke, A. D. *J. Phys. Chem.*, **1993**, *98*, 5648.

[48] Lee, C.; Yang, W.; Parr, R. G. *Phys. Rev. B*, **1988**, *37*, 785.

[49] Hehre, W.J.; Ditchfield, R.; Pople, J. A. *J. Chem. Phys.*, **1972**, *56*, 2257.

[50] Weigend, F.; Haeser, M. *Theo. Chem. Acc.*, **1997**, *97*, 331.

[51] Weigend, F.; Haeser, M.; Patzelt, H.; Ahlrichs, R. *Chem. Phys. Lett.*, **1998**, *294*, 143.

[52] Kendall, R. A.; Dunning, T. H.; Harrison, R. J. *J. Chem. Phys.*, **1992**, *96*, 6796.

[53] Herbert, J. M.; Head-Gordon, M. *J. Phys. Chem. A*, **2005**, *109*, 5217.

[54] Gaussian 03, Revision C.02, Frisch, M. J.; Trucks, G. W.; Schlegel, H. B.; Scuseria, G. E.; Robb, M. A.; Cheeseman, J. R.; Montgomery, Jr., J. A.; Vreven, T.; Kudin, K. N.; Burant, J. C.; Millam, J. M.; Iyengar, S. S.; Tomasi, J.; Barone, V.; Mennucci, B.; Cossi, M.; Scalmani, G.; Rega, N.; Petersson, G. A.; Nakatsuji, H.; Hada, M.; Ehara, M.; Toyota, K.; Fukuda, R.; Hasegawa, J.; Ishida, M.; Nakajima, T.; Honda, Y.; Kitao, O.; Nakai, H.; Klene, M.; Li, X.; Knox, J. E.; Hratchian, H. P.; Cross, J. B.; Bakken, V.; Adamo, C.; Jaramillo, J.; Gomperts, R.; Stratmann, R. E.; Yazyev, O.; Austin, A. J.; Cammi, R.; Pomelli, C.; Ochterski, J. W.; Ayala, P. Y.; Morokuma, K.; Voth, G. A.; Salvador, P.; Dannenberg, J. J.; Zakrzewski, V. G.; Dapprich, S.; Daniels, A. D.; Strain, M. C.; Farkas, O.; Malick, D. K.; Rabuck, A. D.; Raghavachari, K.; Foresman, J. B.; Ortiz, J. V.; Cui, Q.; Baboul, A. G.; Clifford, S.; Cioslowski, J.; Stefanov, B. B.; Liu, G.; Liashenko, A.; Piskorz, P.; Komaromi, I.; Martin, R. L.; Fox, D. J.; Keith, T.; Al-Laham, M. A.; Peng, C. Y.; Nanayakkara, A.; Challacombe, M.; Gill, P. M. W.; Johnson, B.; Chen, W.; Wong, M. W.; Gonzalez, C.; and Pople, J. A.; Gaussian, Inc., Wallingford CT, 2004.

[55] Ahlrichs, R.; Bär, M.; Häser, M.; Horn, H.; Kölmel, C. *Chem. Phys. Lett.* **1989**, *162*, 165.

[56] Straatsma, T.P.; Apr, E.; Windus, T.L.; Bylaska, E.J.; de Jong, W.; Hirata, S.; Valiev, M.; Hackler, M.; Pollack, L.; Harrison, R.; Dupuis, M.; Smith, D.M.A; Nieplocha, J.; Tipparaju V.; Krishnan, M.; Auer, A.A.; Brown, E.; Cisneros, G.; Fann, G.; Frchtl, H.; Garza, J.; Hirao, K.; Kendall, R.; Nichols, J.; Tsemekhman, K.; Wolinski, K.; Anchell, J.; Bernholdt, D.; Borowski, P.; Clark, T.; Clerc, D.; Dachsel, H.; Deegan, M.; Dyall, K.; Elwood, D.; Glendening, E.; Gutowski, M.; Hess, A.; Jaffe, J.; Johnson, B.; Ju, J.; Kobayashi, R.; Kutteh, R.; Lin, Z.; Littlefield, R.; Long, X.; Meng, B.; Nakajima, T.; Niu, S.; Rosing, M.; Sandrone, G.; Stave, M.; Taylor, H.; Thomas, G.;

van Lenthe, J.; Wong, A.; Zhang, Z.; NWChem, A Computational Chemistry Package for Parallel Computers, Version 4.6 (2004), Pacific Northwest National Laboratory, Richland, Washington 99352-0999, USA. Kendall, R.A.; Apr, E.; Bernholdt, D.E.; Bylaska, E.J.; Dupuis, M.; Fann, G.I.; Harrison, R.J.; Ju, J.; Nichols, J.A.; Nieplocha, J.; Straatsma, T.P.; Windus, T.L.; Wong, A.T. *Computer Phys. Comm.*, **2000**, *128*, 260.

[57] Humphrey, W.; Dalke, A.; Schulten, K. *J. Molec. Graphics* **1996**, *14*, 33.

[58] Laaksonen, L. *J. Mol. Graph.* **1992**, *10*, 33.

[59] Bergman, D. L.; Laaksonen, L.; Laaksonen A. *J. Mol. Graph. Model.* **1997**, *15*, 301.

[60] Cornell, W. D.; Cieplak. P.; Bayly, C. I.; Gould, I. R.; Merz, K. M.; Ferguson, D. M.; Spellmeyer, D. C.; Fox, T.; Caldwell, J. W.; Kollman, P. A. *J. Am. Chem. Soc.*, **1996**, *118*, 2309.

[61] Tuttle, T. R.; Golden, S. J.; *J. Phys. Chem.*, **1991**, *95*, 5725.

[62] Jou, F.-Y.; Freeman, G. R. *J. Phys. Chem.*, **1979**, *83*, 2383.

[63] Jungwirth, P.; Tobias, D. J. *J. Phys. Chem. B*, **2002**, *106*, 6361.

[64] Harris, F. J. *Proc. IEEE*, **1978**, *66*, 51.

[65] Chipman, D. M.; *J. Phys. Chem.* , **1978**, *82*, 1080.

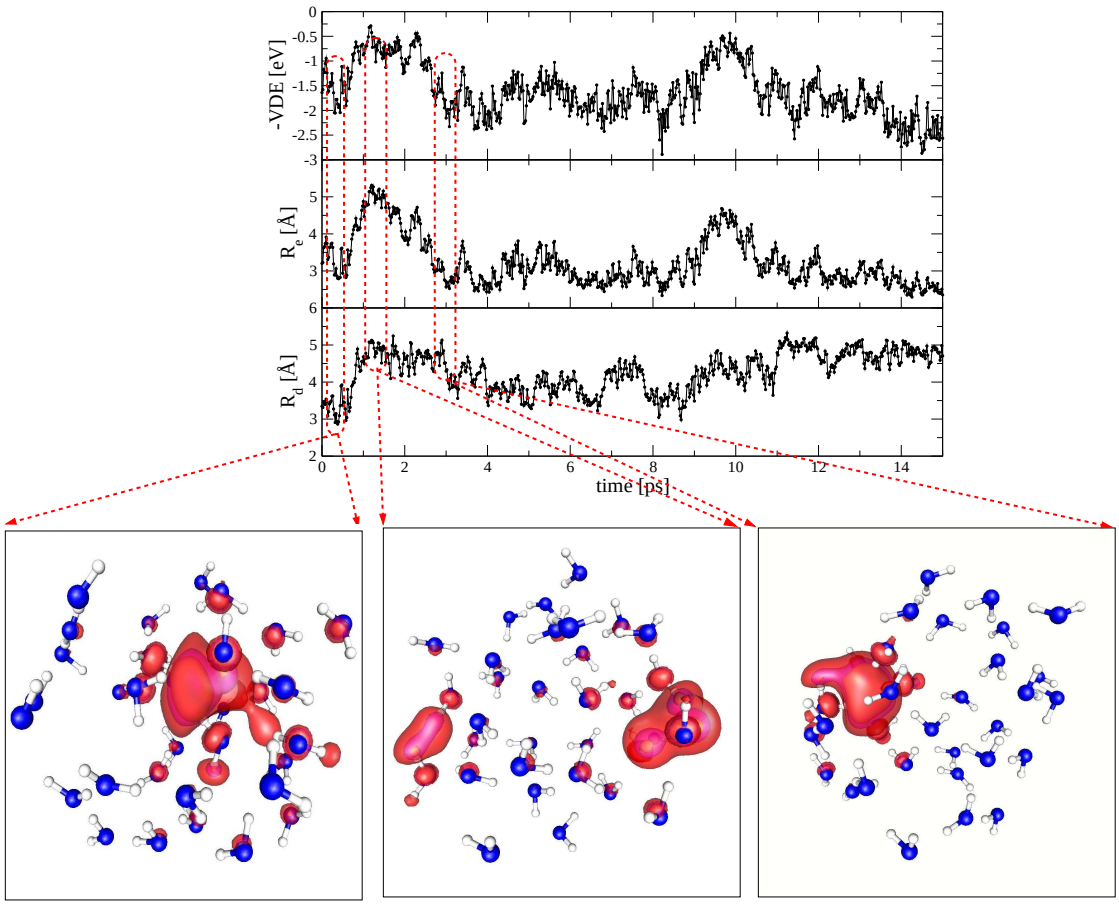

Figure 1: Top panel: electron vertical detachment energies VDEs. Middle panel: electron radius of gyration R_e. Lower panel: mean distance between the excess electron center and the cluster geometrical center R_d. All data are computed at the PBE-GTH-m-TZV2P level. Below the graph the spin density isosurfaces (orange=0.003, magenta=0.002, red=0.001) are shown, at t=0.16 ps, t=1.5 ps and t=3 ps from left to right.

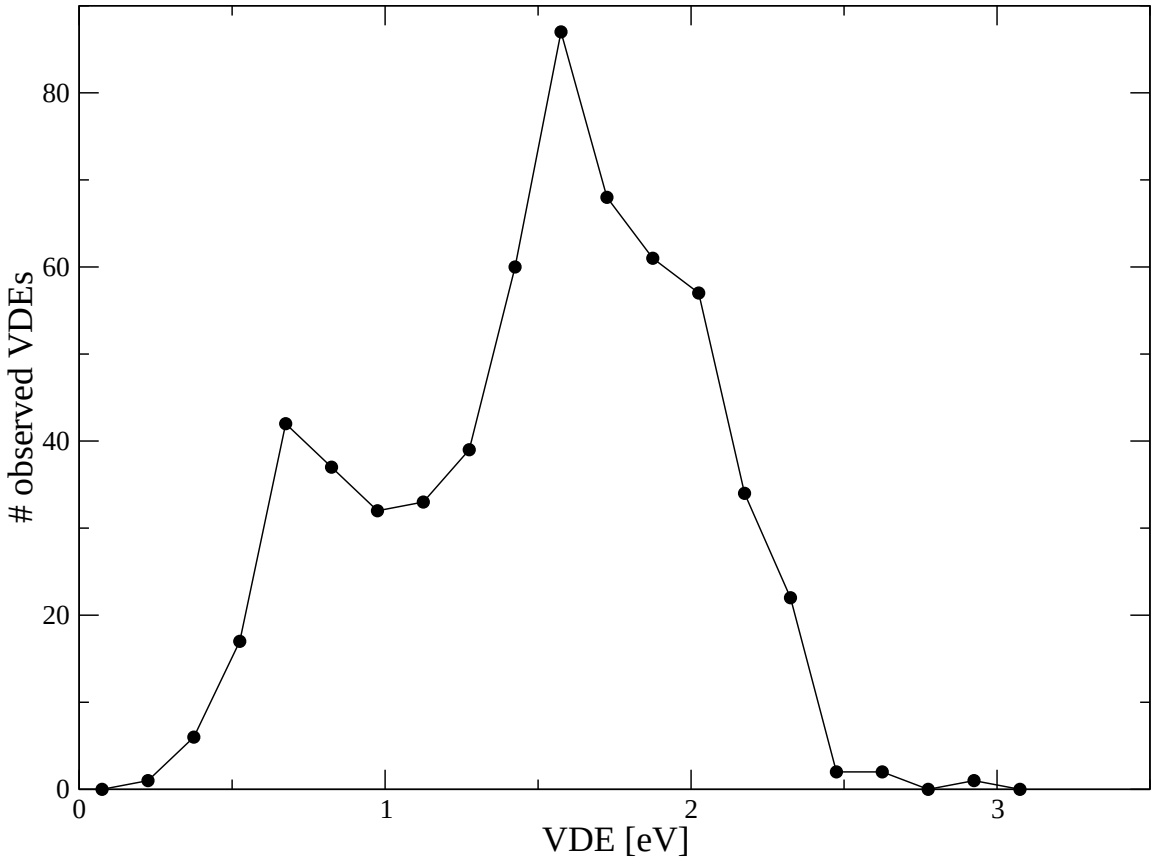

Figure 2: VDE spectrum, computed from the time series shown in Fig. 1.

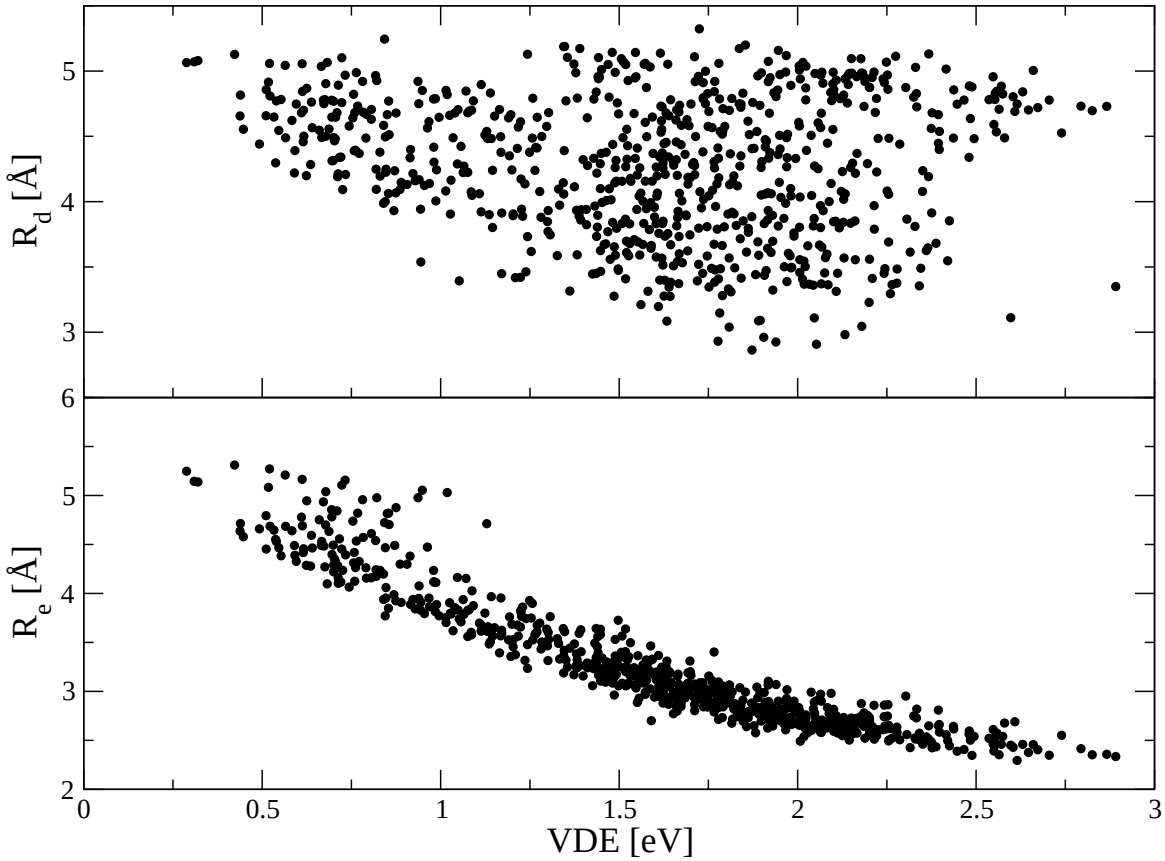

Figure 3: Top panel: correlation between VDE and electron position R_d. Lower panel: correlation between VDE and electron radius of gyration R_e.

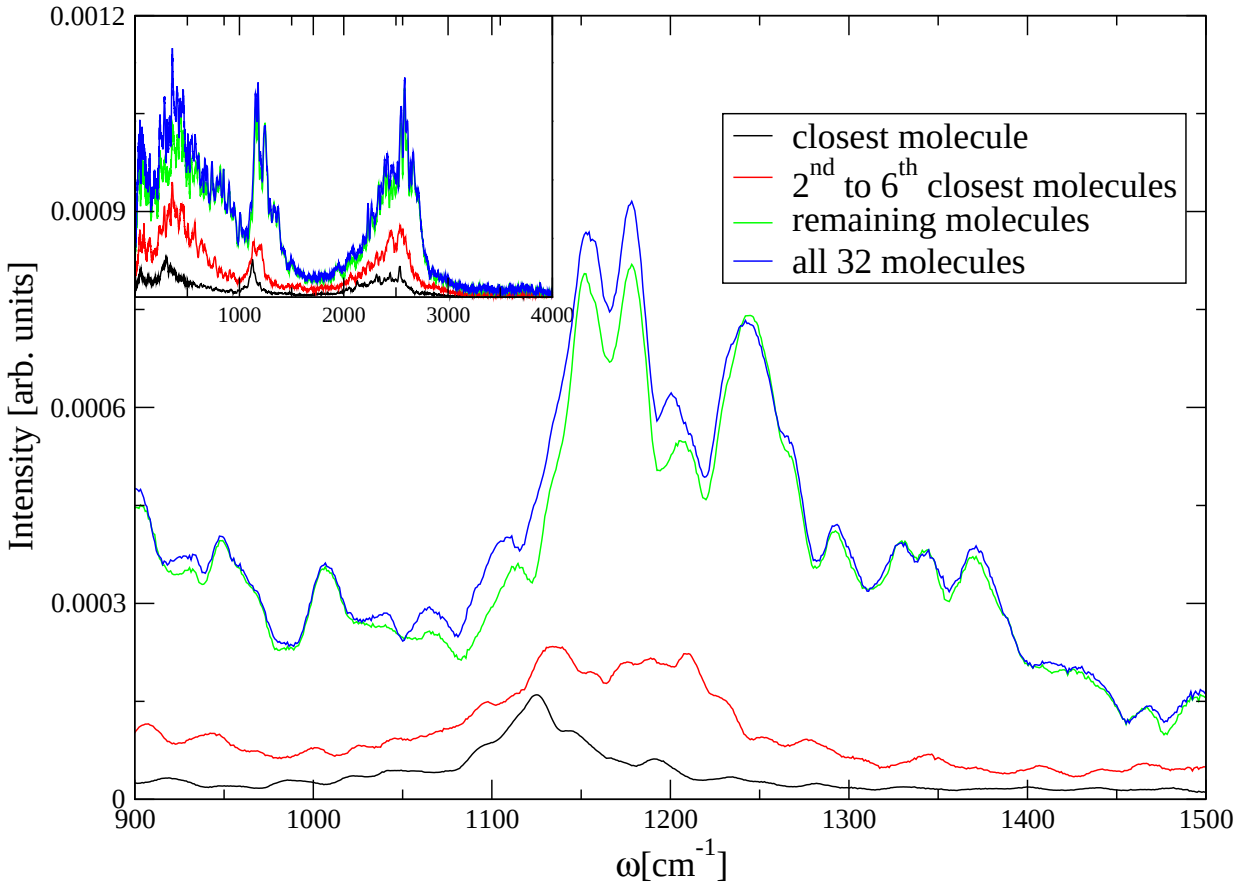

Figure 4: Bending region of the $(H_2O)_{32}^-$ IR spectrum, computed as the Fourier transform of the velocity autocorrelation function extracted from the MD trajectory. Inset: complete IR spectrum. Three IR spectra are added, obtained from: velocities of the water molecule closest to e_{aq}^-, velocities of the 2^{nd} to 6^{th} closest molecules, velocities from the remaining 26 molecules.

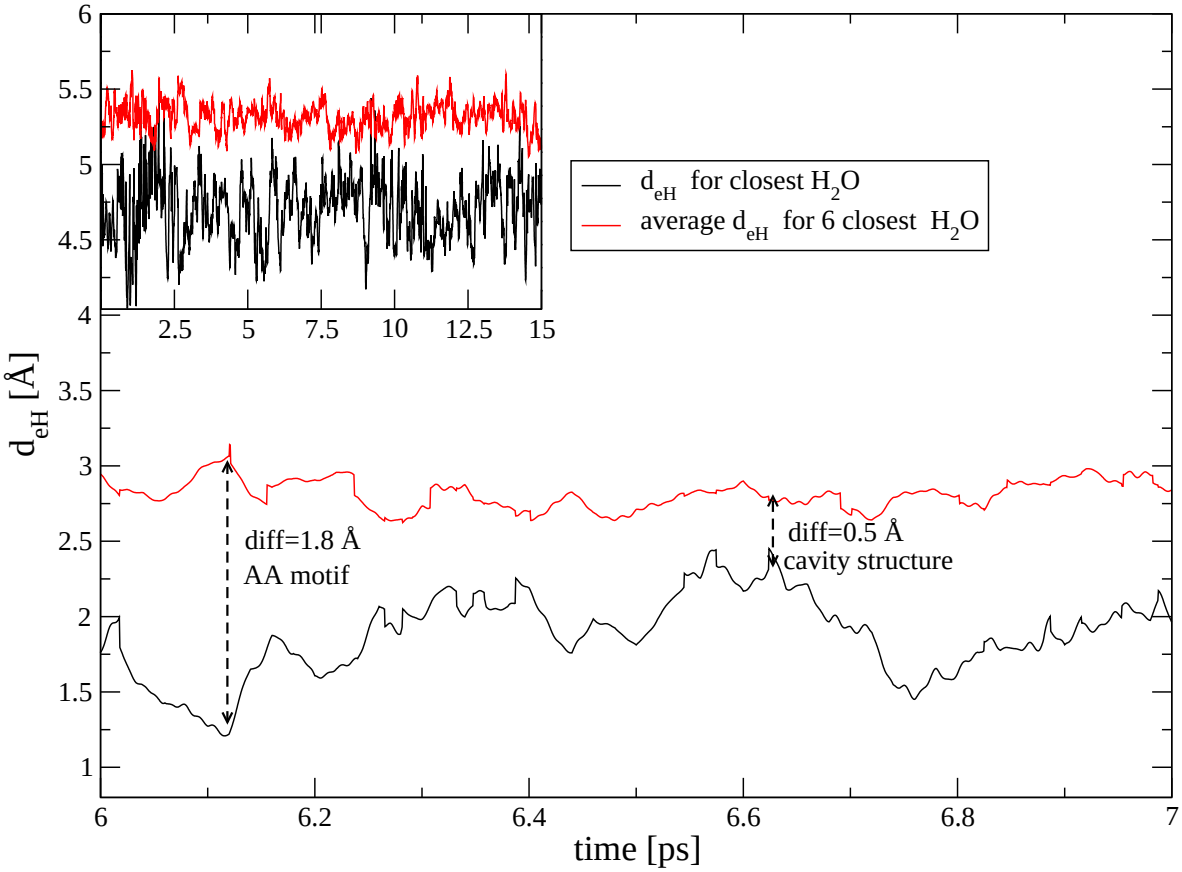

Figure 5: Average $e^-_{aq}\cdots$H distance for molecule closest to e^-_{aq}, and six closest molecules to e^-_{aq}. Inset: complete time series.

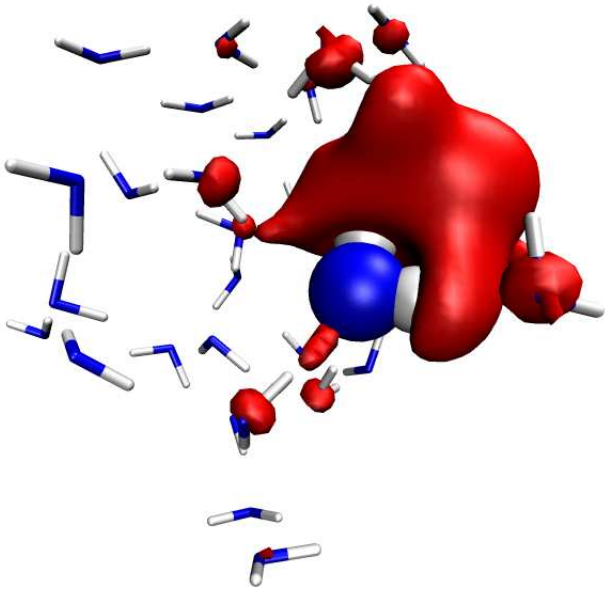

Figure 6: Total spin density (isovalue=0.001) at t=6.12 ps. The single water molecule with both H atoms pointing towards the electronic density, typical of the AA motif, is marked by drawing its atoms as spheres, while other molecules are depicted with a licorice model.

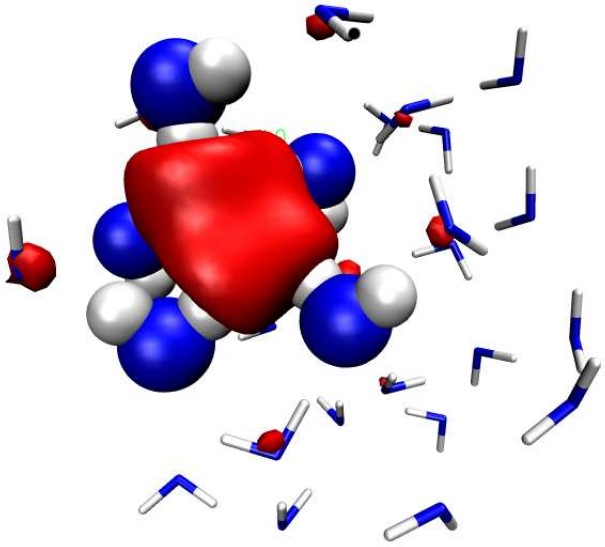

Figure 7: Total spin density (isovalue=0.001) at t=6.62 ps. The molecules closest to e^-_{aq} are marked by drawing their atoms as spheres, while other molecules are depicted with a licorice model.

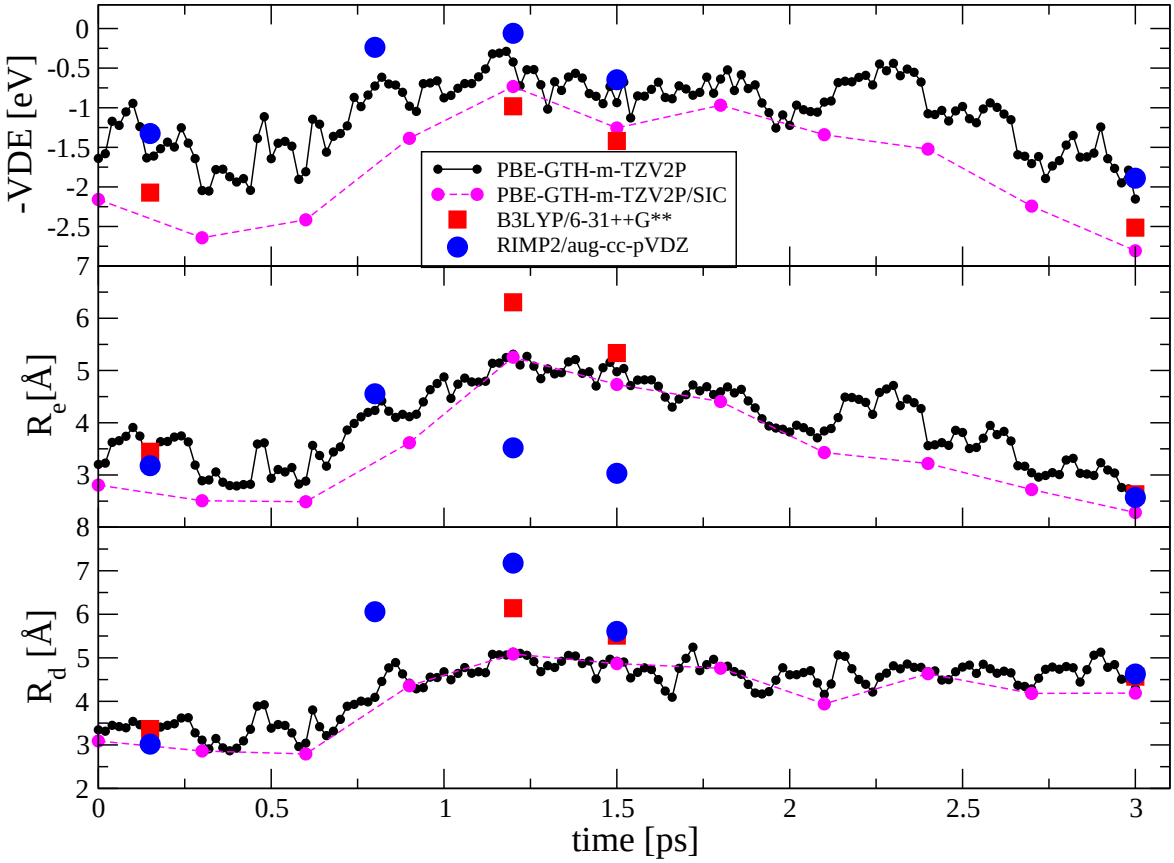

Figure 8: From top to bottom panel: VDEs, electron radius of gyration R_e, mean distance between the excess electron center and the cluster geometrical center R_d. Quantities are computed at different levels of theory, as indicated in the graph legend.

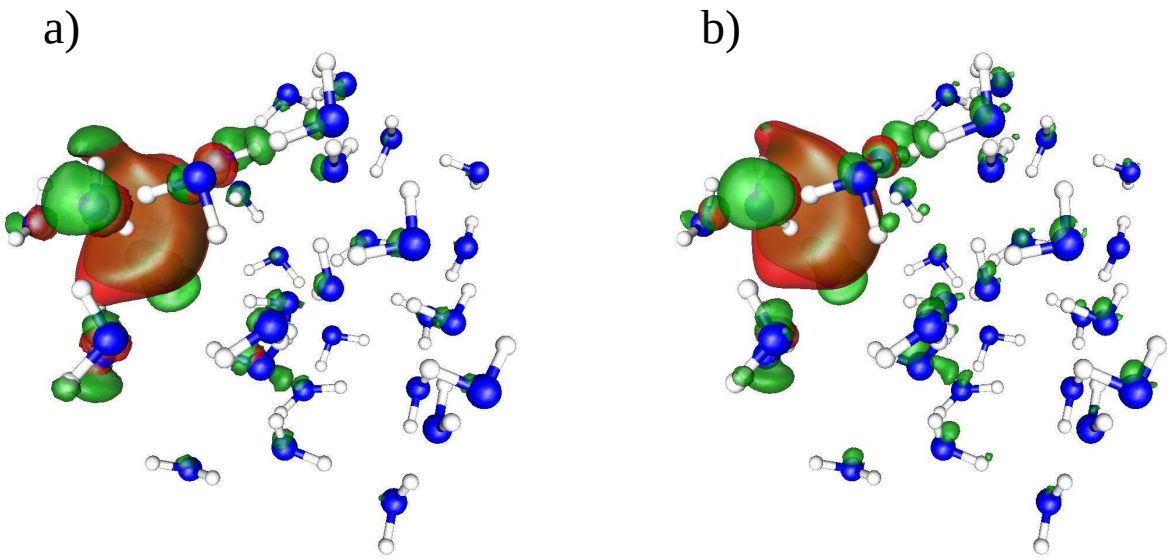

Figure 9: Spin density (red) and differential electronic density (green), at a) PBE-GTH-m-TZV2P and b) RIMP2 level, at a 0.002 isovalue. Note the almost perfect overlap between the spin and differential electronic density for the main lobe and the slightly more diffuse character of the latter.